Lasers in Manufacturing Conference 2019

Metal powder cross-contaminations in multi-material laser powder bed fusion: Influence of CuCr1Zr particles in AlSi10Mg feedstock on part properties

Max Horn[a*], Georg Schlick[a], Max Lutter-Guenther[a], Christine Anstaett[a], Christian Seidel[a,b], Gunther Reinhart[a,c]

[a]*Fraunhofer Research Institution for Casting, Composite and Processing Technology IGCV, Beim Glaspalast 5, 86153 Augsburg, Germany*
[b]*Department of Mechanical, Automotive and Aeronautical Engineering of Munich University of Applied Sciences, Lothstr. 34, 80335 Munich, Germany*
[c]*Institute for Machine Tools and Industrial Management of Technical University of Munich, Boltzmannstr. 15, 85748 Garching b. München, Germany*

Abstract

Metal powder cross-contaminations occurring in multi-material laser powder bed fusion (MMLPBF) are one of the major inhibitors for this novel additive manufacturing technology. In order to evaluate the criticality of named cross-contaminations for a key material combination to be processed by MMLPBF, this study investigates the effects of CuCr1Zr foreign particles in AlSi10Mg feedstock on metallurgical and mechanical properties. Three powder contamination grades ranging from 0.5 to 5.0 weight percent CuCr1Zr are processed and compared with uncontaminated powder feedstock. Metallurgical structure of contaminated samples shows characteristic coppery enclosures. X-ray diffraction analysis indicates the formation of Al_2Cu for increased foreign particle concentrations. Tensile strength tests reveal that this leads to overall material embrittlement and decreased levels of ultimate tensile strength. Based on presented results, critical degrees of contamination for given material combination are discussed. Furthermore, general reusability of the powder materials as well as application possibilities for in-situ alloying are addressed.

Keywords: laser powder bed fusion; multi-material solutions; powder quality; contamination; foreign particles; AlSi10Mg; CuCr1Zr

* Corresponding author. Tel.: +49 (0) 821 90678-187; Fax: +49 (0) 821 90678-199.
E-mail address: max.horn@igcv.fraunhofer.de.

1. Introduction

Reasons to join Aluminum (Al) and Copper (Cu) alloys are versatile. High electric conductivity of both materials combined with high specific strength of Aluminum make the couple a key material combination for e.g., components in high performance electric engines. Rising Cu prices and a better density-to-strength ratio of Al drive the substitution of Cu parts by Al (German Copper Alliance 2009; Hofmann et al. 2014). This could help to manufacture lightweight electric components with increased performance at lower cost. Higher part performance however is also driven by improved electric motor design. Established production technologies that enable joining the two material systems or processing them simultaneously are limited or lack geometrical freedom. Ongoing research in the field of welding, foremost friction stir welding, meanwhile enables resilient material joints (e.g., Hofmann et al. 2014). Additive manufacturing, especially laser powder bed fusion (LPBF), meanwhile successfully processes both materials separately. Due to novel developments in multi-material LPBF (MMLPBF) (e.g., Anstaett et al. 2016, 2017, 2018; Wei et al. 2018) this production technique could become a key technology to manufacture complex parts from Al and Cu base alloys in a single process. Despite the need for further developments in process control, such as powder deposition and process parametrization, the mixing of both materials during the process is a major challenge for quality control of final parts (Vaezi et al. 2013). Horn et al. (2018) investigated the effects of Cu alloy foreign particles in Al alloy matrix on metallurgical structure. The influence of found and characterized defects on part properties however is currently unclear. Thus, this investigation aims at describing the influence of Cu alloy contaminations on tensile strength of Al alloy specimens.

2. Basic principles and literature review

2.1. Multi-material processing of Aluminum and Copper alloys

In accordance with DIN EN ISO ASTM 52900 laser powder bed fusion is an AM technology where a laser is used as energy source to fuse selected regions of a powder bed to form final parts. One main advantage of the process is its high degree of freedom in terms of part geometry and process control. Ongoing research aims at enhancing these possibilities by adding a second or even more materials to the process chamber enabling full MMLPBF capabilities (Anstaett et al. 2016, 2017, 2018; Anstaett and Seidel 2016; Chivel 2016; Ott 2012; Wei et al. 2018). First developments, of which Vaezi et al. (2013) give an overview, allowed to change between materials in the build direction which yielded sandwich-like structures. More recent research allows materials to be switched within one build layer. Due to difficulties in joining Al and Cu base alloys by conventional methods (Galvão et al. 2011; Kaspar et al. 2014) and limited geometrical freedom, novel MMLPBF technologies could become an alternative to create complex parts of named materials. Sing et al. (2015) who used LPBF to create bimetallic laminates of Al alloy AlSi10Mg and Cu alloy C18400 have shown the general applicability of MMLPBF. Examined specimens yielded good metallic continuity between the two material systems. Appearance of the intermetallic compound Al_2Cu in the transition area however, leads to material embrittlement. Tensile strength tests revealed that failure occurs predominately in the Copper areas which lead to the conclusion that the material bond is stronger than the Copper alloy itself. Three point bending tests showed that up to flexural strain of 10 % the two material systems were not separated. Instead, cracks occurred similarly in the Al and Cu matrices showing that material resistance against delamination is higher than individual ultimate flexural strength of both alloys. In contrast to creating discrete material transitions, Wang et al. (2018) used five different Al-Cu-metal-powder-mixtures ranging from 4.5 to 40 weight percent (wt.%) Cu in Al for in-situ alloying. The researchers also observed an increase in Al_2Cu content in the Al matrix from 10 wt.% to 77 wt.% which lead to an inhomogeneous metallic

structure with Al-, Cu- and Al_2Cu-rich micro areas. Rising Al_2Cu content caused material embrittlement and increased compressive strength. In contrast to processing defined material mixtures or combinations as described by the two previously mentioned studies, undesired material contaminations can occur for two reasons in MMLPBF. Firstly, during the process if the material deposition system is not perfectly selective (Horn et al. 2018; Vaezi et al. 2013). Secondly, during the powder recycling in the post process if the MMLPF material mix is not fully separated (Horn et al. 2018; Sing et al. 2015). Therefore, the next subchapter summarizes findings about metal powder cross contaminations in LPBF.

2.2. Metal powder cross contaminations in laser powder bed fusion

Compared to previously mentioned findings, contaminations to be addressed in this study are undesired and degrees of contamination are usually low. Unfortunately, only few detailed studies exist on the effects of foreign particles on base material matrix and its structure as listed by Horn et al. (2018). Often observed defects are cracks and delamination. Jamshidinia et al. (2016) for example found Tungsten (W) particles to cause delamination of Inconel 625 samples above a certain contamination degree. Foreign particles mainly formed unmelted discrete inclusions that significantly weakened the matrix material by lack-of-fusion defects. Kilburn (2016) observed an unknown amount of Ni-base alloy 2.4668 (Inconel 718) particles to cause cracks and delamination of AlSi10Mg. Despite the high difference in melting temperatures, foreign particles were fully melted and formed the brittle $NiAl_3$ and $AlNi_3$ phases that eventually caused part failure. For the same material combination Lutter-Günther et al. (2016) found 1 wt.% Ni-base alloy 2.4668 to form characteristic swirly enclosures in the AlSi10Mg matrix. However, no cracking occurred. Brandão et al. (2017) examined the effects of W particles in Ti6Al4V. Foreign particles remained unmelted in the Titanium matrix. Although not causing any cracks or lack-of-fusion defects in the samples, the W enclosures served as preferred sites of crack initiation, which lead to decreased fracture elongation. Referring to the material combination to be addressed in this paper, Horn et al. (2018) found foreign particles of Cu base alloy CuCr1Zr to be fully melted and form characteristic enclosures in an AlSi10Mg matrix comparable to defects previously described by Lutter-Günther et al. (2016). Three transition zones between CuCr1Zr particles and the Al matrix were identified, where a eutectic structure of primary Al and Al_2Cu was the predominant phase. It was also found that the number of defects rose with increased contamination levels. The general shape and appearance of enclosures however remained constant. Repeated remelting of coppery enclosures during the LPBF process leads to wider distribution of the foreign material into the matrix and thus more creation of Al_2Cu.

For Al Cu cross-contaminations, current knowledge about resulting material properties is limited to flexural and tensile strength of discrete transition zones (Sing et al. 2015) as well as compressive strength of processed powder mixtures with high degrees of contamination (Wang et al. 2018). Implications of defects described by Horn et al. (2018) on material strength are currently missing and are therefore be investigated in this study.

3. Materials and methods

3.1. Materials

For the underlying application of high performance electric components, the Cu alloy should serve as functional material for e.g., electricity or heat conduction. The Al alloy should mainly serve as structural material and bear the main share of loads. Thus, in this study, the influence of Cu alloy particles in Al alloy feedstock was investigated and the following materials were chosen.

The Al alloy EN AC-43000, which is referred to as AlSi10Mg, serves as matrix material. It is a hardenable cast alloys that shows good electric conductivity as well as high chemical stability in corrosive atmospheres (DIN EN 1706:2013). Due to its good processability in LPBF combined with high specific strength it is the currently most common Al alloy for this AM process (SLM Solutions 2019). Metal powder from SLM Solutions Group AG with the specification +20/-63 µm was used for the underlying study. The Cu alloy CW106C, which is referred to as CuCr1Zr, was chosen as contamination material. Adding Chromium (Cr) and Zirconium (Zr) to the Cu matrix increases material strength as well as heat and wear resistance without significantly lowering its heat and electric conductivity (German Copper Alliance 2005). Powder with a specification of +20/-45 µm was supplied by Schmelzmetall GmbH. Table 1 shows particle sizes measured with a Masersizer 3000 from Malvern Panalytical Ltd. For both materials.

Table 1. Particle sizes of the used powder materials

Material	$d_{10,3}$ in µm	$d_{50,3}$ in µm	$d_{90,3}$ in µm
CuCr1Zr (CW106C)	21	40	70
AlSi10Mg (EN AC-43000)	20	32	45

The binary Al-Cu-system shows a large number of intermetallic compounds. Technical relevance however is limited to both ends of the binary system. Up to 15 wt.% Al is used as main alloying element in Cu material systems to increase tensile strength, fracture elongation and hardness (German Copper Alliance 2010). Cu on the other hand is the main alloying element in the 2xxx-series of Al alloys and enables precipitation hardening. Al can solve up to 5.56 wt.% of Cu, forming a solid solution. Above this concentration the hard and brittle θ (Al_2Cu) intermetallic compound starts to form precipitations (Macherauch and Zoch 2011). The Al-Cu binary system shows an eutectic at 32.7 wt.% Cu (Murray 1985). At 53.5 wt.% Cu the binary system only consists of Al_2Cu. Between this value and 87.2 wt.% Cu in Al a number of technically less relevant intermetallic compounds occur (Murray 1985).

3.2. Experimental procedure

In order to secure comparability with structural defects characterized by Horn et al. (2018), the same contamination levels were chosen. As qualitative differences between 0.5 wt.% and 1 wt.% were negligible, the latter level was excluded from this investigation. Thus, 0.5 wt.% 3 wt.% and 5 wt.% were examined. The two powders were mixed and manually tumbled. Powder mixtures were processed on a SLM 250 ^{HL} LPBF machine from SLM Solutions Group AG. Cubes with a dimension of 10 x 10 x 10mm^3 were manufactured and cut in x-y- and y-z-planes for X-ray diffraction analysis (XRD) using a PANalytical X'Pert PRO MRD diffractometer facilitating a θ-2θ-geometry and Cu-Kα-radiation. The Reference Intensity Ratio (RIR) method was used for semi-quantitative phase identification. Furthermore, a minimum of three tensile strength rods per orientation (0°, 45° and 90°) and degree of contamination were produced according to DIN 50125 – B4 x 20. Tensile strength test were conducted on a UPM 50 kN machine from ZwickRoell in accordance with DIN EN ISO 6892-1. Specimens that broke close to the thread were excluded from the analysis in order to only include specimens where the elongation could be measured correctly. This was true for four specimens. However, apart from the 0.5 wt.% CuCr1Zr tensile test rods built upright (0°) a minimum of three specimens were analyzed. Fractography was conducted using a Hitachi TM3030Plus Scanning Electron Microscope (SEM), where backscattered electrons (BSE) were used for compositional analysis and secondary electrons (SE) to acquire topographical information.

4. Results and discussion

4.1. Metallurgical structure

Horn et al. (2018) and Wang et al. (2018) concluded that the Cu alloy powder contaminations in AlSi10Mg mainly lead to an Al_2Cu enrichment and thus an Al-Al_2Cu eutectic structure in the contaminated regions. To further investigate phase formation during LPBF of contaminated powder materials, an XRD analysis was conducted. Figure 1 shows the results for 0 wt.% and 5 wt.% CuCr1Zr contamination. As relevant differences between the two material compositions mainly appear in the area between angles (2θ) of 20° and 50° this section is displayed below (Figure 1). Both graphs show peaks which were identified as Calcium Carbonate ($CaCo_3$) phases. It appears the signal is derived from the compound in which the specimens were embedded. Although Bakelite was used, the semi-quantitative phase matching wrongfully suggested $CaCo_3$ due to material similarities. Thus, the $CaCo_3$ signal is excluded from further analyses.

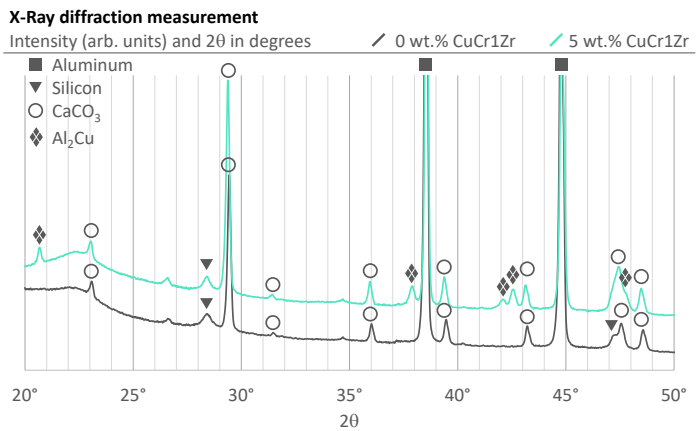

Fig. 1. X-ray diffraction analysis results for pure AlSi10Mg and 0.5 wt.% CuCr1Zr.

The predominant phase for both contamination levels is the primary Al phase with contents of 98 wt.% and 86 wt.% for 0 wt.% and 5 wt.% CuCr1Zr respectively. The Silicon phase increases from 2 wt.% in pure AlSi10Mg to 4 wt.% in 5 wt.% contamination. This growth can be explained by the formation of Al_2Cu which has a share of 10 wt.% in the metallurgical structure of the contaminated specimen. As only Aluminum is consumed during the intermetallic compound creation the relative share of Silicon increases. No further phases were detected which is interesting to that extend that the Al-Cu binary system shows a large number further compounds. The fact that only Al_2Cu was detected leads to the conclusion that either no further phases are formed or their share is below the detection limit of ~1 wt.%. Influence on mechanical part properties however, can be limited mainly to the formation of Al_2Cu inclusions in the α-Aluminum matrix. This Finding helps to better understand implications for material properties as presented in the next chapter.

4.2. Tensile strength

Figure 2 shows the influence of 0.5 wt.%, 3 wt.% and 5 wt.% CuCr1Zr foreign particles on tensile strength R_m, yield strength $R_{p0.2}$ and elongation at fracture A compared to specimens manufactured from pure AlSi10Mg. All graphs show the results as arithmetic mean values for all three build directions (0°, 45° and 90°). In addition, error bars show the standard deviation and solid lines are second-degree polynomials to

depict trends between part property and increasing contamination level. Finally, dashed lines show minimum values for respective properties and part orientation of AlSi10Mg according to VDI3405, Blatt 2.1.

Starting with tensile strength, it stands out that specimens manufactured of uncontaminated AlSi10Mg only just meet or slightly supersede the minimum values of VDI3405. Part density is above 99% and although no virgin powder was used for the underlying experiment previous build jobs were unobtrusive. Despite being improvable, the data can still be used for comparison with contaminated specimens as influences affected all jobs similarly. One finding to address is the noticeable trend. Parts of all build directions face a decrease in tensile strength at 0.5 wt% CuCr1Zr and upright and horizontally built specimens still do at 3 wt.% CuCr1Zr. At 5 wt.% contamination. However, material properties of 0.5 wt.% and/or 3 wt.% contamination respectively are superseded. This can be explained by the formation and of Al_2Cu in respective quantities. Horn et al. (2018) have shown that at 0.5 wt.% foreign particles, unconnected isolated enclosures appear. Whereas at 3 wt.% contamination, Al_2Cu enclosures start to connect and at 5 wt.% a mesh of interconnected swirly enclosures can be observed. Thus, positive effects of conventional precipitation hardening come into effect and material strength starts to increase.

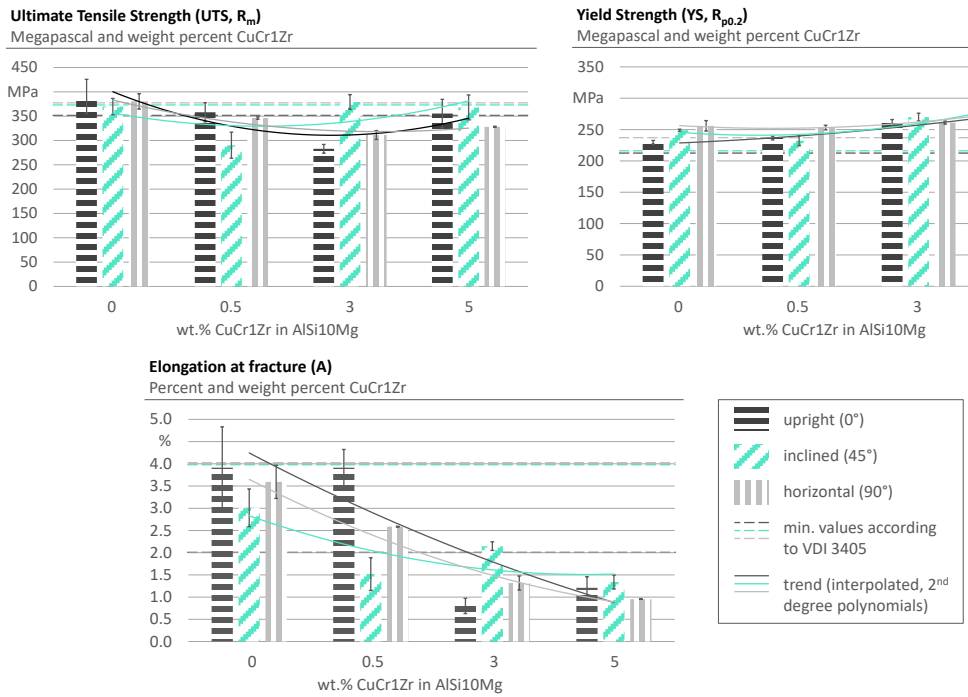

Fig. 2. Tensile strength, yield strength and fracture elongation of different contamination levels and build directions of AlSi10Mg.

These findings are in line with $R_{p0.2}$ yield strength results (Figure 2). For this material property, an upward trend can be observed. Only horizontal and inclined specimens show a slight decrease in yield strength at 0.5 wt.% CuCr1Zr. For higher contamination degrees and all build directions, the material strength increases. In this case, a similar logic as for tensile strength applies. Interconnected larger Al_2Cu enclosures are likely to prevent deformation in the Aluminum matrix and thus increase yield strength. Single isolated conspicuities however seem to have a slight negative effect. It is noteworthy that 3 wt.% CuCr1Zr already seem to have a strictly positive influence on the yield strength for all build directions, which is not true for tensile strength. Described findings are in line with other material systems where certain amounts of precipitates are

necessary to achieve desired material properties. Jägle et al. (2016) found a drop of 0.09 wt.% Scandium (Sc) in Scalmalloy to be accountable for a moderate drop in material strength as less Al_3Sc precipitates developed.

Fracture elongation is also depicted in Figure 2. Again, only one build direction meets minimum values as suggested by VDI3405. High standard deviations and larger measuring inaccuracies below 1.5% elongation at fracture prevent detailed assessments of single build orientations or contamination degrees. The overall trend however seems valid. It is in accordance with previously made assumptions for tensile and yield strength as Al_2Cu enrichment leads to lower fracture elongations and general material embrittlement. For better understanding of the influence of Al_2Cu enrichment on material properties and fracture dynamics, as well as to review previously made assumptions, fracture surfaces were examined in the next chapter.

4.3. Fractography

All fractures are rather brittle with no necking. Inclined (45°) samples have a tendency towards shear fractures (angle of 45°), whereas upright (0°) samples mainly show cleavage fractures (horizontal surface). Horizontally built samples show both directions with a slight tendency towards angled fracture surfaces. As fracture types appear to be systematic, it was concluded that respective types derive from material structure and not from clamping induced shear stresses that can occur during tensile testing. Macroscopic fracture surface appearance and general fracture types are not influenced by the degree of contamination as Figure 3 exemplarily illustrates for 0 wt.% and 3 wt.% CuCr1Zr. It was found that upright samples of all contamination degrees contain melt track remnants, which might indicate bonding defects and in turn explain the tendency towards cleavage fractures. Overall structure however indicates transgranular cleavage or shear fracture with low ductility for all build directions and contamination levels (Figure 3).

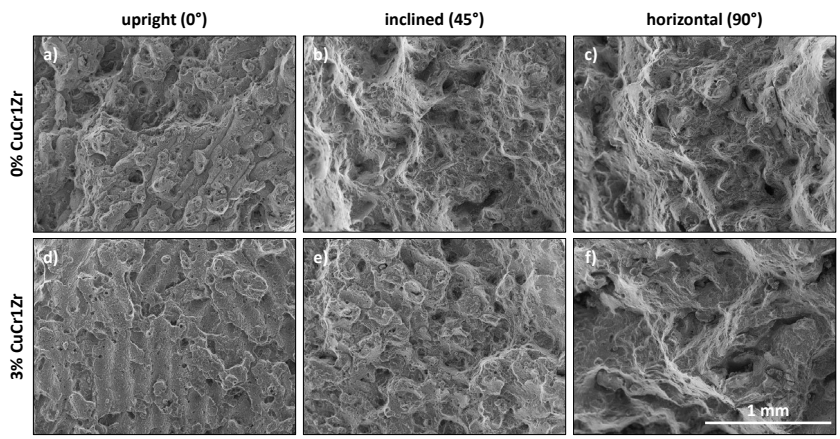

Fig. 3. Overview SEM SE images of 0% (a, b, c) and 3% (d, e, f) Cu alloy contamination of upright (a, d), 45° (b, e) and horizontally (c, f) built specimens.

Figure 4 shows SEM BSE images of 0.5 (a), 3 (b) and 5 (c) wt.% foreign particles. Due to higher material density, coppery enclosures appear brighter and are exemplarily highlighted with circles. In line with findings from Horn et al. (2018) and conclusions from chapter 4.2, at 0.5 wt.% contamination enclosures appear as single isolated defects which are likely to weaken the material. At 3 wt.% conspicuities appear in larger number and start to interconnect. Bright spots however can well be differed. At 5 wt.% only a few single brighter areas are distinguishable. The overall structure appears to have a light bright shimmer indicating

larger areas containing higher amounts of Cu, which stand out less, compared to samples with lower

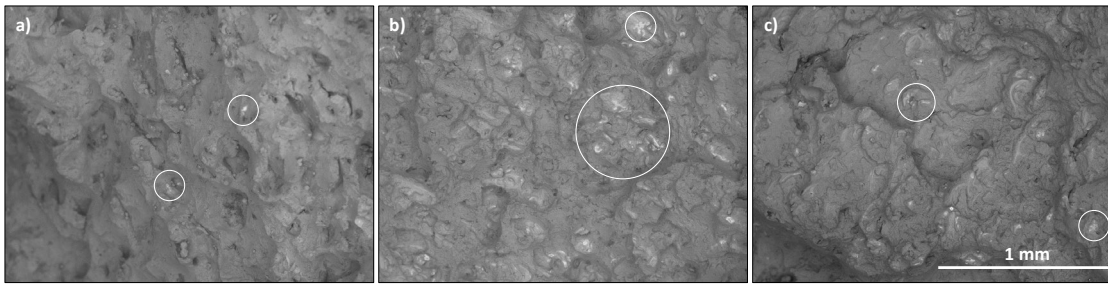

Fig. 4. SEM BSE images inclined (45°) specimens with 0.5% (a), 3% (b) and 5% (c) CuCr1Zr contamination. Coppery enclosures appear brighter due to higher material density (partially and exemplarily marked with circles).

contamination levels.

Exemplary details of foreign particle enclosures are shown in Figure 5, where a) and b) display the top right conspicuity marked in Figure 4 a). Images c) and d) show a detail of an upright specimen containing 3 wt.% CuCr1Zr. Beside the Cu-rich areas marked with ⓪, two of three transition zones identified by Horn et al. (2018) can be identified. Zone ① consists of Al_2Cu-rich hypereutectic material and transitions towards acicular, needle like hypoeutectic material in zone ②, which consists of lamellar eutectic structure in the primary Aluminum matrix. Material composition and its fracture behavior is further illustrated in Figure 5 b).

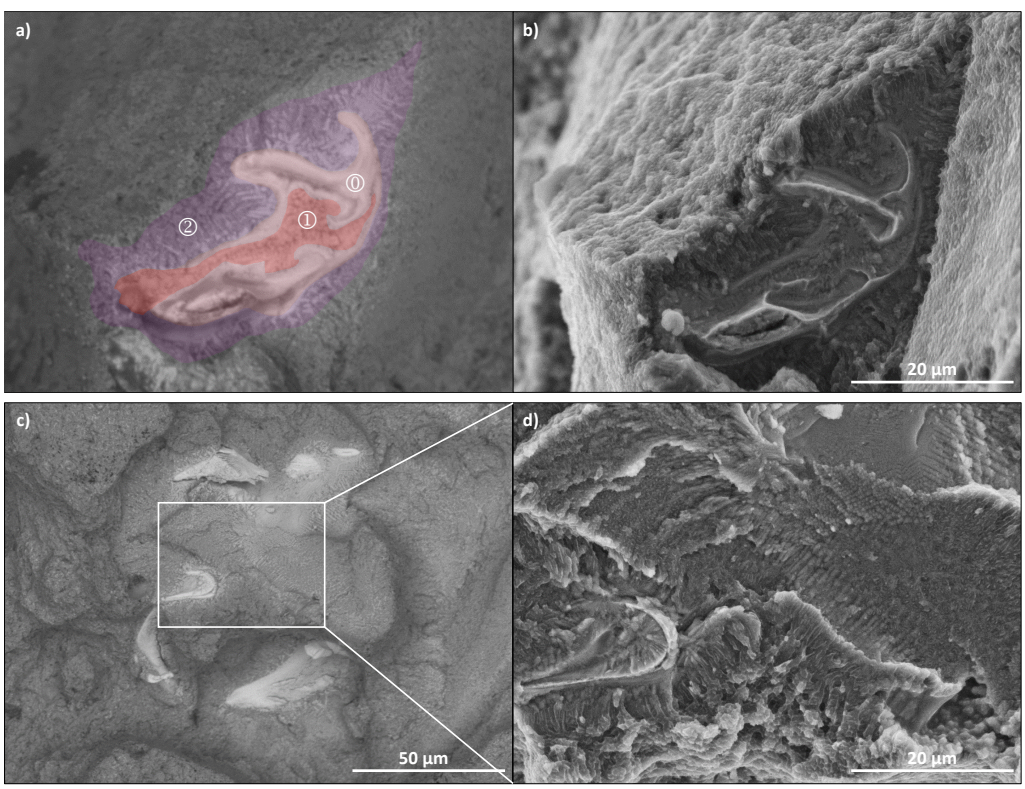

Fig. 5. SEM BSE (a, c) and SE (b, d) images of coppery enclosures found in specimens with 0.5 wt.% contamination (a, b) and 3 wt.% contamination (c, d).

Elevated and smooth surfaces in Cu-rich zone ⓪ might derive from deformation as seen in alloys having higher ductility. However, this is ambiguous as comparably smooth surfaces could also be an indication for microscopic hot cracks in zone ⓪. Zones ① and ② in contrast show brittle cleavage fracture behavior. Around the CuCr1Zr enclosure, characteristic AlSi10Mg honeycombed fracture surface is found. Thus, the isolated foreign particle seems to have limited influence on its surrounding material performance. It appears however, the coppery conspicuity influenced the overall fracture direction. The crack might have moved along the slope ranging from bottom right corner of the image towards the top left corner. The slope is only interrupted by the ledge containing the melted foreign particle. Which leads to the conclusion that the defects can influence fracture propagation and direction. It might also be an indication that hot cracks occurred during solidification.

Images c) and d) of Figure 5 show an exemplary enclosure of a 3 wt.% CuCr1Zr specimen. Although overall defect appearance does not change, as suggested by Horn et al. (2018), light grey areas that can mainly be identified as transition zone ② appear larger. Figure 5 d) displays a magnified detail of the highlighted area. The fracture type in this zone tends to be a brittle cleavage fracture, which suits the primary Al-Al_2Cu eutectic structure and is in line with overall material behavior and strength as described in chapter 4.2.

Altogether, the presented line of argument is a series of contributions to explain the initial decrease in material strength followed by an increase above certain levels of contamination as well as the overall material embrittlement as shown in the tensile strength tests.

5. Conclusion and outlook

In order to investigate the effects of CuCr1Zr foreign particles in AlSi10Mg feedstock during LPBF, XRD measurements were conducted to characterize influence on material composition. In addition, tensile strength tests were executed to investigate impact on material performance. It can be concluded that the contamination mainly leads to formation of the brittle intermetallic compound Al_2Cu. Roughly 10 wt.% of named phase, which were created by adding 5 wt.% of CuCr1Zrto AlSi10Mg metal powder already form a network of enclosures which in turn lead to strong material embrittlement, a slight decrease in tensile strength and a considerable increase in yield strength. Below a certain contamination degree, where foreign material phases are not connected however, the main effect was material weakening. For MMLPBF powder recycling, where levels of contamination below 1 wt.% can be expected, material weakening could be compensated by higher safety factors during part construction – for tensile strength at least. This could still enable high performance electronic multi-material components. Resulting material embrittlement however, could exclude contaminated powders from certain applications. Influence on further material properties, such as fatigue or corrosion resistance, still needs to be investigated. It was also found that the material combination is suitable for in-situ alloying as suggested by Wang et al. (2018). In order to achieve desired effects of alloying during the LPBF process, a minimum contamination level is necessary. For this purpose, it is suggested that heat treatment of in-situ alloyed specimens is included in upcoming investigations. Further diffusion of Cu atoms into the primary Al matrix might lead to lower necessary contamination levels and material homogenization, which might have a positive effect on reproducibility and material reliability.

Acknowledgements

The authors express their sincere thanks to the Freistaat Bayern and its Bavarian Ministry of Economic Affairs, Energy and Technology StMWi for funding the "MULTIMATERIALZENTRUM Augsburg" (English: “Multi-material Center Augsburg”). Furthermore, the authors acknowledge the work of Felix Wegner that contributed to this article and thank Dr. Jan Petersen of Fraunhofer IST, for conducting the XRD analysis.

Finally yet importantly, the corresponding author thanks thank Mario Schafnitzel for the fruitful discussions during the creation of this article.

References

Anstaett, C., & Seidel, C. (2016). Next Step in Laser-Based Powder Bed Fusion - Multi Material Processing. *Laser Technik Journal, 13.*

Anstaett, C., Seidel, C., & Reinhart, G. (2016). Multi-Material Processing in Laser Beam Melting. *Fraunhofer DDMC 2016*.

Anstaett, C., Seidel, C., & Reinhart, G. (2017). Fabrication of 3D Multi-material Parts Using Laser-based Powder Bed Fusion. *Proceedings of the 28th Annual International SFF Symposium*.

Anstaett, C., Seidel, C., & Reinhart, G. (2018). Multi-Material Fabrication of Copper-Chrome-Zirconia and Tool Steel 1.2709 by Powder Bed Based Laser Beam Melting. *Fraunhofer DDMC 2018*.

Brandão, A. D., Gerard, R., Gumpinger, J., Beretta, S., Makaya, A., Pambaguian, L., et al. (2017). Challenges in Additive Manufacturing of Space Parts: Powder Feedstock Cross-Contamination and Its Impact on End Products. *Materials, 10,* (*5*).

Chivel, Y. (2016). New Approach to Multi-material Processing in Selective Laser Melting. *Physics Procedia, 83,* (891–898).

DIN 50125: Testing of metallic materials - Tensile test pieces. Berlin: Beuth 2016.

DIN EN 1706: Aluminium and aluminium alloys - Castings - Chemical composition and mechanical properties. Berlin: Beuth 2013.

DIN EN ISO 6892-1: Metallic materials - Tensile testing: Method of test at room temperature. Berlin: Beuth 2017.

DIN EN ISO ASTM 52900: Additive Manufacturing - General Principles - Terminology. Berlin: Beuth 2015.

Galvão, I., Oliveira, J. C., Loureiro, A., & Rodrigues, D. M. (2011). Formation and distribution of brittle structures in friction stir welding of aluminium and copper: influence of process parameters. *Science and Technology of Welding and Joining, 16,* (*8*, 681–689).

German Copper Alliance. Material data sheet CuCr1Zr. Accessed: 6 June 2018.

German Copper Alliance. (2009). Schweißen von Kupfer und Kupferlegierungen. *Informationsdruck i.12*.

German Copper Alliance. (2010). Cu Al Alloys (3rd Edition). *Informationsdruck i.6*.

Hofmann, K., Holzer, M., Hugger, F., Roth, S., & Schmidt, M. (2014). Reliable Copper and Aluminum Connections for High Power Applications in Electromobility. *Physics Procedia, 56,* (601–609).

Horn, M., Schlick, G., Wegner, F., Seidel, C., Anstaett, C., & Reinhart, G. (2018). Defect formation and influence on metallurgical structure due to powder cross-contaminations in LPBF. *Proceedings of 7th International Conference on Additive Technologies*.

Jägle, E. A., Sheng, Z., Wu, L., Lu, L., Risse, J., Weisheit, A., et al. (2016). Precipitation Reactions in Age-Hardenable Alloys During Laser Additive Manufacturing. *JOM, 68,* (*3*, 943–949).

Jamshidinia, M., Boulware, P., Marchal, J., Mendoza, H., Cronley, L., Kelly, S., et al. (2016). In-Process Monitoring of Cross Contamination in Laser Powder Bed Fusion (L-PBF) Additive Manufacturing (AM). *Proceedings of the 27th Annual International SFF Symposium*.

Kaspar, J., Zimmermann, M., Ostwaldt, A., Goebel, G., Standfuß, J., & Brenner, B. (2014). Challenges in Joining Aluminium with Copper for Applications in Electro Mobility. *Materials Science Forum, 783-786,* (1747–1752).

Kilburn, P. (2016). LPW Technology – Intelligence in Metal. *Company Presentation*. http://www.advantageaustria.org/gb/events/LPWTechnologies_PhilKilburn_3011_2.pdf. Accessed: 25 May 2018.

Lutter-Günther, M., Schwer, F., Seidel, C., & Reinhart, G. (2016). Effects on Properties of Metal Powders for Laser Beam Melting Along the Powder Process Chain. *Fraunhofer DDMC 2016*.

Macherauch, E., & Zoch, H.-W. (Eds.). (2011). *Praktikum in Werkstoffkunde. 91 ausführliche Versuche aus wichtigen Gebieten der Werkstofftechnik* (11th Edition). Wiesbaden: Vieweg+Teubner.

Murray, J. L. (1985). The aluminium-copper system. *International Metals Reviews, 30,* (*1*, 211–234).

Ott, M. (2012). *Laser beam and powder bed based multi-material additive manufacturing process*. (Dissertation, Technical University of Munich). https://mediatum.ub.tum.de/node?id=1095129.

Sing, S. L., Lam, L. P., Zhang, D. Q., Liu, Z. H., & Chua, C. K. (2015). Interfacial characterization of SLM parts in multi-material processing: Intermetallic phase formation between AlSi10Mg and C18400 copper alloy. *Materials Characterization, 107,* (220–227).

SLM Solutions. (2019). Material Data Sheet Al-Alloy AlSi10Mg / EN AC-43000 / EN AC-AlSi10Mg, 190201-AlSi10Mg.

Vaezi, M., Chianrabutra, S., Mellor, B., & Yang, S. (2013). Multiple material additive manufacturing – Part 1: a review. *Virtual and Physical Prototyping, 8,* (*1*, 19–50).

VDI 3405, Blatt 2.1: Additive manufacturing processes, rapid manufacturing - Laser beam melting of metallic parts; Material data sheet aluminium alloy AlSi10Mg. Düsseldorf: Beuth 2015.

Wang, P., Deng, L., Prashanth, K. G., Pauly, S., Eckert, J., & Scudino, S. (2018). Microstructure and mechanical properties of Al-Cu alloys fabricated by selective laser melting of powder mixtures. *Journal of Alloys and Compounds, 735,* (2263–2266).

Wei, C., Li, L., Zhang, X., & Chueh, Y.-H. (2018). 3D printing of multiple metallic materials via modified selective laser melting. *CIRP Annals.*